Constant-Depth Circuits for Dynamic Simulations of Materials on Quantum Computers

Lindsay Bassman,[1] Roel Van Beeumen,[1] Ed Younis,[1] Ethan Smith,[2] Costin Iancu,[1] and Wibe A. de Jong[1]

[1] *Lawrence Berkeley National Lab, Berkeley, CA 94720*
[2] *University of California Berkeley, Berkeley, CA 94720*

Dynamic simulation of materials is a promising application for noisy intermediate-scale quantum (NISQ) computers. The difficulty in carrying out such simulations is that a quantum circuit must be executed for each time-step, and in general, these circuits grow in size with the number of time-steps simulated. NISQ computers can only produce high-fidelity results for circuits up to a given size due to gate error rates and qubit decoherence times, limiting the number of time-steps that can be successfully simulated. Here, we present a method for producing circuits that are constant in depth with increasing simulation time-steps for dynamic simulations of quantum materials for a specialized set of Hamiltonians derived from the one-dimensional Heisenberg model. We show how to build the constant-depth circuit structure for each system size N, where the number of CNOT gates in circuit grows only quadratically with N. The constant-depth circuits, which comprise an array of two-qubit matchgates on nearest-neighbor qubits, are constructed based on a set of multi-matchgate identities that we introduce as conjectures. Using our constant-depth circuits, we are successfully able to demonstrate long-time dynamic simulations of quantum systems with up to five spins on available quantum hardware. Such constant-depth circuits could enable simulations of long-time dynamics for scientifically and technologically relevant quantum materials, enabling the observation of interesting and important atomic-level physics.

I. INTRODUCTION

While a quantum advantage was recently achieved with random circuits [1], it remains a challenge to demonstrate a quantum advantage for an application of interest within the physical sciences, a feat which has been dubbed "physical quantum advantage". This is because current and near-term quantum computers, otherwise known as noisy intermediate-scale quantum (NISQ) computers [2], have low qubit counts and suffer from short qubit decoherence times and high gate error rates, making it difficult to perform relevant, large-scale computations. Given such constraints, long-anticipated applications like number factorization [3] and unordered database search [4] are still far out of reach for NISQ computers. Quantum computers, however, are intrinsically fit for efficiently simulating quantum systems [5–8], making the dynamic simulation of quantum materials a leading "killer application" for NISQ computers. Rapid progress in both quantum hardware and software may soon allow for such simulations to not only demonstrate a physical quantum advantage, but to advance such fields as condensed matter physics, quantum chemistry, and materials science.

One of the major challenges with performing dynamic simulations on NISQ devices is keeping the quantum circuits small enough to produce high-fidelity results. Dynamic simulations require the execution of one circuit per time-step, where each circuit implements the time-evolution operator from the initial time to the given time-step [9]. Current algorithms for dynamic materials simulations produce quantum circuits whose depths grow with increasing simulation time-steps [10, 11]. Thus, an essential part of the workflow for simulating the dynamics of materials on NISQ computers is quantum circuit optimization, which can minimize the depth of the circuits produced by current algorithms. Already, a great deal of research has focused on general circuit optimization (i.e. minimization) [12–19], and domain-specific circuit optimizers, which focus on optimizing certain types of circuits for specific applications, have been suggested [20] as a method to reduce to complexity of the optimization problem, which in general is NP-hard [21, 22].

According to the "no-fast-forwarding theorem", simulating the dynamics of a system under a generic Hamiltonian H for a time t requires $\Omega(t)$ gates [23, 24], implying that circuit depths grow at least linearly with the number of time-steps. It has been shown, however, that quadratic Hamiltonians can be fast forwarded, meaning the evolution of the systems under such Hamiltonians can be simulated with circuits whose depths do not grow significantly with the simulation time [25]. A recent work took advantage of this to variationally compile approximate circuits with a hybrid classical-quantum algorithm for fast-forwarded simulations [26]. The circuits, however, are approximate, with error that grows with increasing fast-forwarding time.

Here, we present a method for producing quantum circuits that are constant in depth with increasing simulated time-steps for simulations of materials whose dynamics are governed by specialized models derived from the Heisenberg Hamiltonian, which we denote by $\mathcal{H}_{\mathcal{CD}}$ and define in Section II. The circuits are comprised of two-qubit gates, known as matchgates [27]. While generic matchgates decompose into native-gate circuits with three CNOT gates [28], the matchgates for Hamiltonians in $\mathcal{H}_{\mathcal{CD}}$, have the special property that they only require two CNOT gates in their decomposition. This special property allows us to introduce a set of conjectured matchgate identities, which enable the downfolding of our circuits for dynamic simulations into constant-

depth for any number of time-steps.

The constant-depth circuits have a fixed structure, with only the single-qubit rotation parameters changing with the addition of more time-steps. The circuits are exact up to Trotter error, which can be made arbitrarily small since the constant-depth nature of the circuits allows for the simulation to be broken into arbitrarily many time-steps. Furthermore, the circuit structure has a regular pattern which can be easily extrapolated to build circuits for any system size. The number of CNOT gates for the constant-depth circuit for a system of size N scales quadratically with N. For a given system size, if the fixed circuit structure is small enough to achieve high-fidelity results on a NISQ computer, the dynamics of that system can be successfully simulated out to arbitrarily long times. By removing the limit on the number of simulation time-steps, these constant-depth circuits allow for long-time dynamic simulations that can give insights into complex molecular reactions, transformations, and equilibration.

II. THEORETICAL BACKGROUND

The quantum circuits for dynamic simulations of quantum materials must implement the time-evolution operator between the initial time (which we set to 0) and some final time t, given by

$$U(0,t) \equiv U(t) = \mathcal{T}\exp(-i\int_0^t H(t)dt) \tag{1}$$

where $\mathcal{T}$ indicates a time-ordered exponential and $H(t)$ is the time-dependent Hamiltonian of the material. In general, this operator is challenging to compute exactly due to the time-dependence of the Hamiltonian and the exponentiation the Hamiltonian. First, an approximation must be made which transforms $H(t)$ into a piece-wise function by discretizing time into small time-steps over which $H(t)$ is constant [29]. For small system sizes, it is then possible to compute $U(t)$ by exact diagonalization of the Hamiltonian, however, this task becomes exponentially harder with increasing system size. Thus for larger system sizes, a second approximation must be made to exponentiate the Hamiltonian. Typically, the Trotter decomposition [30] is used, which splits the Hamiltonian into components that are each easy to diagonalize. With these two approximations, the time-evolution operator becomes

$$U(n\Delta t) = \prod_{\tau=1}^{n}\prod_{l} e^{-iH_l(t_\tau)\Delta t} + \mathcal{O}(\Delta t) \tag{2}$$

where τ multiplies over the number of discretized time-steps Δt and l multiplies over the components into with $H(t)$ was divided.

The constant-depth circuits we introduce here simulate the dynamical evolution of a quantum material whose Hamiltonian is a simplified version of the one-dimensional (1D) Heisenberg model, as explained below. The Heisenberg Hamiltonian is defined as

	J_x	J_y	J_z	J_x+J_y	J_x+J_z	J_y+J_z	$J_x+J_y+J_z$
x	×	×	×			×	
y	×	×	×		×		
z	×	×	×	×			
$\varnothing$	×	×	×	×	×	×	

TABLE I. Subsets of Heisenberg parameters $\mathcal{H}_{\mathcal{CD}}$ for which circuits are constant-depth. The rows denote the direction of the external field or a lack of a field. The columns denote the non-zero coupling parameters. Table entries marked with an × denote parameter sets that represent Hamiltonians for which our constant-depth circuits work.

$$H(t) = -\sum_{\alpha}\{J_\alpha\sum_{i=1}^{N-1}\sigma_i^\alpha\sigma_{i+1}^\alpha\} - h_\beta(t)\sum_{i=1}^{N}\sigma_i^\beta \tag{3}$$

where α sums over $\{x,y,z\}$, the coupling parameters J_α denote the exchange interaction between nearest-neighbor spins along the α-direction, σ_i^α is the α-Pauli matrix acting on qubit i, and $h_\beta(t)$ is the time-dependent amplitude of an external magnetic field along the β-direction, where $\beta \in \{x,y,z\}$. This Hamiltonian is thus defined by the set of its parameters $\{J_x, J_y, J_z, h_\beta(t)\}$. We denote the set of all parameter sets as $\mathcal{H}$. The full Heisenberg model is obtained when all parameters in the set are non-zero, however a number of ubiquitous models can be derived by setting various parameters to zero.

Table I shows all subsets $\mathcal{H}_{\mathcal{CD}}$ of $\mathcal{H}$ for which we find that our constant-depth circuits work. The rows of the table denote either the direction of the external magnetic field h_β or a lack of field, while the columns label which of the coupling parameters are non-zero. The first three columns denote parameter sets where one coupling term is non-zero, the next three columns denote sets where two coupling terms are non-zero, while the final column denotes the sets where all three coupling parameters are non-zero. An × appears in table entries for parameter sets that define Hamiltonians in $\mathcal{H}_{\mathcal{CD}}$, which can be simulated with our constant-depth circuits. Note that $J_x \cdot J_y \cdot J_z = 0$ is a necessary but not sufficient condition for constant-depth. As all $\mathcal{H}_{\mathcal{CD}}$ Hamiltonians of Table I are quadratic, it is possible to fast-forward simulations under their time-evolution [25]. In Section IV, we demonstrate simulations with our constant-depth circuits for two important models in $\mathcal{H}_{\mathcal{CD}}$: (i) the XY model, where $J_z = 0$ and $h_\beta = 0$, and (ii) the transverse field Ising model (TFIM), where $J_y = J_z = 0$. Dynamics of these models have recently been simulated on quantum computers, but lack of constant-depth circuits either limited the number of time-steps that could be successfully simulated [11].

III. CONSTRUCTION OF CONSTANT-DEPTH CIRCUITS

To arrive at the circuit structure for the constant-depth circuits, we begin by laying down the gates that implement evolution of the system by one time-step, $U(\Delta t)$. Due to the quadratic nature of $\mathcal{H}_{\mathcal{CD}}$ Hamiltonians, which only contain coupling interactions between nearest neighbor spins, the circuit for evolution of one time-step can be constructed by a set of two-qubit gates which act on each of the pairs of nearest neighbor qubits. For example, for six qubits, this circuit is given by

$U(\Delta t) =$ 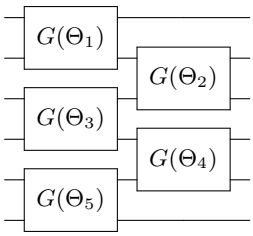

(4)

where each gate labeled $G(\Theta_i)$ is a two-qubit gate defined by some set of parameters Θ_i. For ease of notation, the parameter set Θ_i is dropped in subsequent labeling of these gates, which will simply be labeled with a G. However, it must be emphasized that each two-qubit gate has its own unique parameter set. Each additional time-step requires one additional repetition of the circuit for one time-step. In this manner, it is possible to construct circuits for dynamic simulations that grow with increasing numbers of time-steps. We refer to these circuits has the "naive circuits" for dynamic simulations. The naive circuit for n time-steps for six qubits is thus given by

$U(n\Delta t) =$ 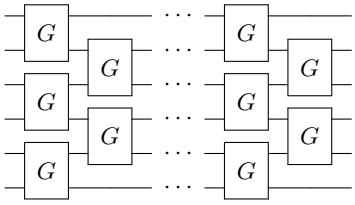

(5)

where there are $2n$ columns of G gates for n time-steps. We now show that it is possible to reduce the naive circuits for higher numbers of time-steps down to a constant-depth circuit which is comprised of N columns of G gates for an N-spin system, where each column alternates placing the top of the first G gate on the first or second qubit. The ability to "downfold" longer circuits into constant-depth circuits is derived from special properties of these G gates.

In fact, the G gates belong to a special group of two-qubit gates known as matchgates [27].

Definition 1. *Let the matrices A and B be in $SU(2)$*

$$A = \begin{bmatrix} p & q \\ r & s \end{bmatrix}, \qquad B = \begin{bmatrix} w & x \\ y & z \end{bmatrix}, \tag{6}$$

with $\det(A) = \det(B)$. Then the two-qubit matchgate $G(A,B)$ is defined as follows

$$G(A,B) = \begin{bmatrix} p & & & q \\ & w & x & \\ & y & z & \\ r & & & s \end{bmatrix}. \tag{7}$$

Matchgates have the important property that the product of two matchgates is again a matchgate and will be a key feature to arrive at constant-depth circuits.

Lemma 2. *Let $G(A_1,B_1)$ and $G(A_2,B_2)$ be matchgates, then the matrix*

$$G(A_3,B_3) = G(A_1,B_1)\,G(A_2,B_2), \tag{8}$$

is again a matchgate with $A_3 = A_1A_2$ and $B_3 = B_1B_2$.

Proof. The proof directly follows from carrying out the matrix-matrix multiplication. □

A graphical representation of Lemma 2 is given by

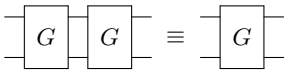

(9)

The decomposition of a general matchgate into a native-gate circuit, which can be executed on NISQ devices, requires three CNOT gates [28]. However, all the matchgates for $\mathcal{H}_{\mathcal{CD}}$ have a special structure which allows them to be decomposed into native-gate circuits with only two CNOT gates. In $\mathcal{H}_{\mathcal{CD}}$ cases with an external magnetic field along the x- or y-directions, the gates G in (4) do not have the matchgate structure but are spectrally equivalent with a matchgate and are in fact matchgates up to some $\pi/2$ rotations. Matchgates and their corresponding decomposition into native-gate circuits with two-CNOTs are given in Appendix A.

The ability to contract the circuits to constant depth relies on an identity that we conjecture for these special $\mathcal{H}_{\mathcal{CD}}$ matchgates.

Conjecture 3. *Let G_1, G_2, G_3 be matchgates of a certain type in $\mathcal{H}_{\mathcal{CD}}$, then there exist three corresponding matchgates G_4, G_5, G_6 of the same type so that*

$$(G_1 \otimes I)(I \otimes G_2)(G_3 \otimes I) = (I \otimes G_4)(G_4 \otimes I)(I \otimes G_6). \tag{10}$$

A graphical representation of Conjecture 3 is given by

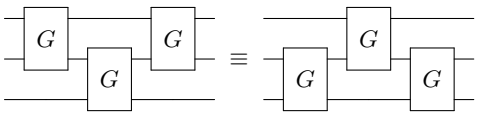

(11)

Using numerical optimization to identify circuit parameters on either side of the equality, we empirically find this conjecture to be true for all trials where the circuits are comprised of $\mathcal{H}_{\mathcal{CD}}$ matchgates. It has, however, proven challenging to analytically compute the parameters of the circuit on the right-hand side given the parameterized circuit on the left-hand side and vice versa.

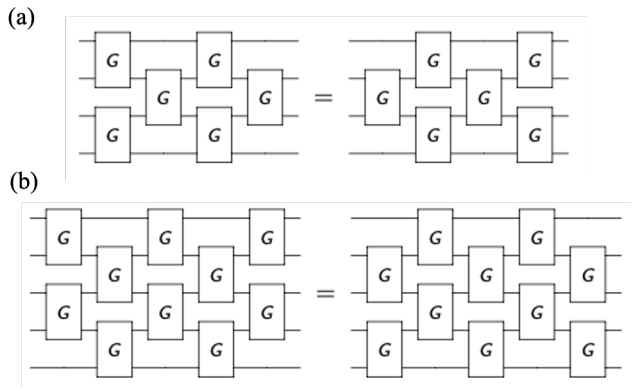

FIG. 1. Conjectured $\mathcal{H}_{\mathcal{CD}}$ matchgate mirroring identities for four qubits (a) and for five qubits (b).

As a result, compilation of our constant-depth circuits requires numerical optimization to obtain circuit parameters. We emphasize that the equivalence (11) only holds for $\mathcal{H}_{\mathcal{CD}}$ matchgates, whereas the equivalence (9) holds for all matchgates.

Based on Eqs. (9) and (11) we can derive identities for higher numbers of qubits, where a set of N columns of matchgates across N qubits can be replaced by its mirror image, albeit with altered parameter sets for all the constituent matchgates. A demonstration of deriving the identity for 4-qubits is shown in Appendix B. We refer to these identities as the matchgate mirroring identities. These conjectured identities are depicted in Fig. 1 for four and five qubits. Note that for even numbers of qubits the mirroring is about a vertical axis (Fig. 1a), while for odd numbers of qubits the mirroring is about a horizontal axis (Fig. 1b). We emphasize that the matchgate parameters are different on either side of the equality signs.

To understand how these mirroring identities allow for the construction of constant depth circuits, we notice that for an N-qubit naive circuit (e.g., Eq. (5)) we can apply the matchgate mirroring identity to the last N columns of matchgates in the circuit. We emphasize that applying this identity will change the parameters defining each matchgate within the mirroring group. Application of this identity will result in pairs of adjacent matchgates on the same qubit pairs that can be combined into one matchgate, thus reducing the number of columns of matchgates in the circuit by one. This can be repeated until only N columns of matchgates in the circuit remain. This process is demonstrated for six qubits in Fig. 2. Fig. 2a shows the naive circuit for six qubits simulating n time-steps with the last six columns of matchgates in the circuit highlighted with an outline. Fig. 2b shows one application of the matchgate mirroring identity for six qubits to these last six columns of matchgates. Note how after applying the identity, two pairs of matchgates emerge adjacent to one another on the same pair of qubits, highlighted with an outline. These pairs can each be merged into one matchgate with new parameters, thus reducing the number of columns of matchgates in the circuit by one. This process is repeated until only six columns of matchgates remain, as shown in Fig. 2c.

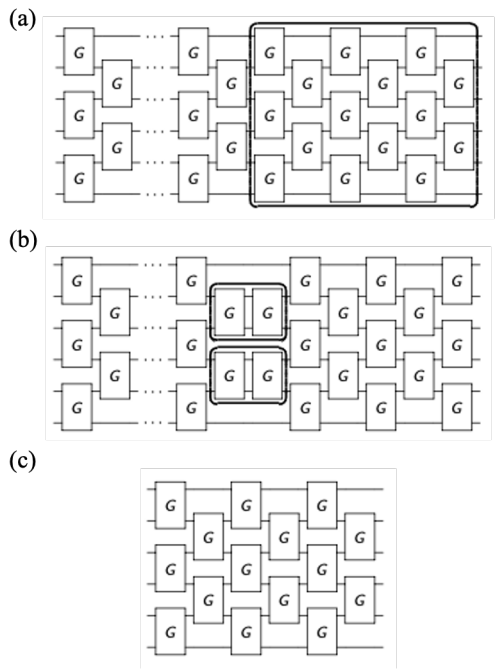

FIG. 2. Downfolding a 6-qubit circuit for n time-steps down to a constant-depth circuit. (a) The 6-qubit circuit for evolving the system by n time-steps with the time-evolution operator $U(n\Delta t)$. A box highlights the last six columns of matchgates to which the matchgate mirroring identity will be applied. (b) The 6-qubit circuit after application of the $\mathcal{H}_{\mathcal{CD}}$ matchgate mirroring identity. Pairs of adjacent matchgates on the same qubit pairs which can be combined into one matchgate with new parameters are highlighted with an outline. (c) The final constant-depth circuit for a 6-qubit circuit, which has six columns of matchgates.

The downfolding approach presented in Fig. 2 shows how to methodically obtain constant-depth circuits for each time-step in the dynamic simulation. In practice, however, we directly use numerical optimization to find the parameters for the constant-depth circuit of Fig. 2c. We begin by computing the operator in Eq. (2) (either by exact diagonalization or Trotter decomposition), which defines our target matrix (i.e., the matrix our circuit aims to carry out). Given a system size, we then construct the constant-depth circuit structure, which has N columns of matchgates for an N-qubit system. Next, we compute the matrix equivalent of the circuit, which will be compared to our target matrix. Using numerical optimization, we then solve for the parameters of the circuit that minimize the distance between the circuit matrix and the target matrix.

The number of circuit parameters grows quadratically with system size. This makes scaling to larger system sizes challenging as the circuit optimization for each time-step will take longer to compute. This could be

ameliorated by finding a way to map the coefficients of the Hamiltonian directly to the rotation angles in the constant-depth circuit, whether through analytical techniques or machine learning methods. This would enable one to skip computation of the time-evolution operator and numerical optimization altogether. It should be noted, however, that the inability to remove this classical optimization step may not completely inhibit this method because the constant-depth circuit generation is embarrassingly parallel. In other words, the circuits for each time-step may all be computed in parallel, as numerical optimization for one circuit does not depend on information from any other circuit. In this way, the numerical optimization of circuits for all time-steps for large system simulations could be executed simultaneously on a classical supercomputer, which are regularly used for similar computations.

The volume of the constant-depth circuits grows quadratically with system size N, while the depth grows only linearly with N. We emphasize, however, that unlike previous circuit generation techniques, our circuits do not grow in size with increasing numbers of time-steps, but rather remain fixed for a given system size N. This remarkable feature is what enables simulation out to arbitrarily large numbers of time-steps and thus permits long-time dynamic simulations. Most other methods for circuit generation will produce circuits that grow linearly with increasing numbers of time-steps [10, 11]. This prohibits dynamic simulations beyond a certain number of time-steps due to the quantum computer encountering circuits that are too large, and thus accumulate too much error due to gate errors and qubit decoherence.

IV. RESULTS

To demonstrate the power of our constant-depth circuits, we simulate quantum quenches of 3-, 4-, and 5-spin systems defined by the TFIM and XY model on the IBM quantum processor "ibmq_athens". A quantum quench is simulated by initializing the system in the ground state of an initial Hamiltonian, H_i, and then evolving the system through time under a final Hamiltonian, H_f. Quenches can simulate a sudden change in a system's environment and provide insights into the non-equilibrium dynamics of various quantum materials.

To obtain the TFIM, we set $J_y = J_z = 0$ and $\beta = z$ in the Hamiltonian in Eq. (3). To perform the quench, we assume the external magnetic field is initially turned off, and the qubits are initialized in the ground state of an initial Hamiltonian $H_i(t<0) = \sum_i -J_x\,\sigma_i^x\sigma_{i+1}^x$, which is a ferromagnetic state oriented along the x-axis. At time $t = 0$, a time-dependent magnetic field is instantaneously turned on, and the system evolves under the final Hamiltonian $H_i(t \geq 0) = -\sum_i \{J_x\sigma_i^x\sigma_{i+1}^x + h_z(t)\sigma_i^z\}$. We use parameters from Ref [31], setting $J_x = 11.83898\,\text{meV}$ and $h_z(t) = 2J_x\cos(\omega t)$ with $\omega = 0.0048\,\text{fs}^{-1}$, which simulates a simplified model of a Re-doped mono-layer of $MoSe_2$ under laser excitation. A time-step of 3 fs is used in the simulations. Our observable of interest is the average magnetization of the system along the x-axis, given by $m_x(t) = \frac{1}{N}\sum_i \langle\sigma_i^x(t)\rangle$.

To obtain the XY model, we set $J_z = h_\beta = 0$ in the Hamiltonian in Eq. (3). To perform the quench, we assume $J_x = J_y = -1.0\,\text{eV}$ and let $J_z \to \infty$, resulting in an initial Hamiltonian $H_i(t<0) = C\sum\sigma_i^z\sigma_{i+1}^z$, where C is an arbitrarily large constant. The ground state of this Hamiltonian is the Néel state, defined as $|\psi_0\rangle = |\uparrow\downarrow\uparrow\cdots\downarrow\rangle$. At time $t = 0$, we instantaneously set $J_z = 0$, giving a final Hamiltonian of $H_f(t \geq 0) = \sum_i\{\sigma_i^x\sigma_{i+1}^x + \sigma_i^y\sigma_{i+1}^y\}$. A time-step of 0.025 fs is used in the simulations. Our observable of interest is the staggered magnetization of the system, which is related to the antiferromagnetic order parameter and given by $m_s(t) = \frac{1}{N}\sum_i(-1)^i\langle\sigma_i^z(t)\rangle$.

To generate the constant-depth circuits for our simulations, we rely on circuit optimization software provided by the circuit synthesis toolkit BQSKit [32]. This suite of software provides several packages which can be used to generate the constant-depth circuits. The user must provide the matrix representation for the time-evolution operator to be implemented along with the parameter-dependent constant-depth circuit structure. The circuit synthesis software then proceeds to use numerical optimization to find the optimal parameters for the circuit.

Fig. 3 shows the simulation results for quenches of the TFIM (top row) and XY model (bottom row) for various system sizes. In the first three columns, the results from our constant-depth circuits (red) and IBM-compiled circuits (green) are compared to the expected results computed with a noise-free quantum computer simulator (blue). The x-axis gives the number of simulation time-steps, while the y-axis gives the time-dependent observable. Circuits from the IBM compiler, as well as other state-of-the-art general purpose compilers, grow in depth with increasing numbers of time-steps. For this reason, the IBM-compiled circuits produce qualitatively consistent results for the first few time-steps, but thereafter the circuits are too large, accumulating too much error, to produce reliable results. A recent benchmark study of dynamic simulations of similar systems on quantum computers found analogous behavior, with high-fidelity results limited to only a handful of time-steps [11]. In contrast, the results from our constant-depth circuits remain accurate for all time-step counts, and in principle, will remain so out to arbitrarily many time-steps. These results thus show the power of constant-depth circuits to enable long-time dynamic simulations.

Fig. 3d and 3h compare the number of CNOT gates for each time-step in the constant-depth (red) and IBM-compiled (green) circuits for 3- (dotted line), 4- (dashed lined), and 5-spin (solid line) systems. Clearly the number of CNOT gates remains the same for all time-steps for our constant-depth circuits, but the number grows linearly with increasing numbers of time-steps for the IBM-compiled circuits. Notice how the number of CNOT gates

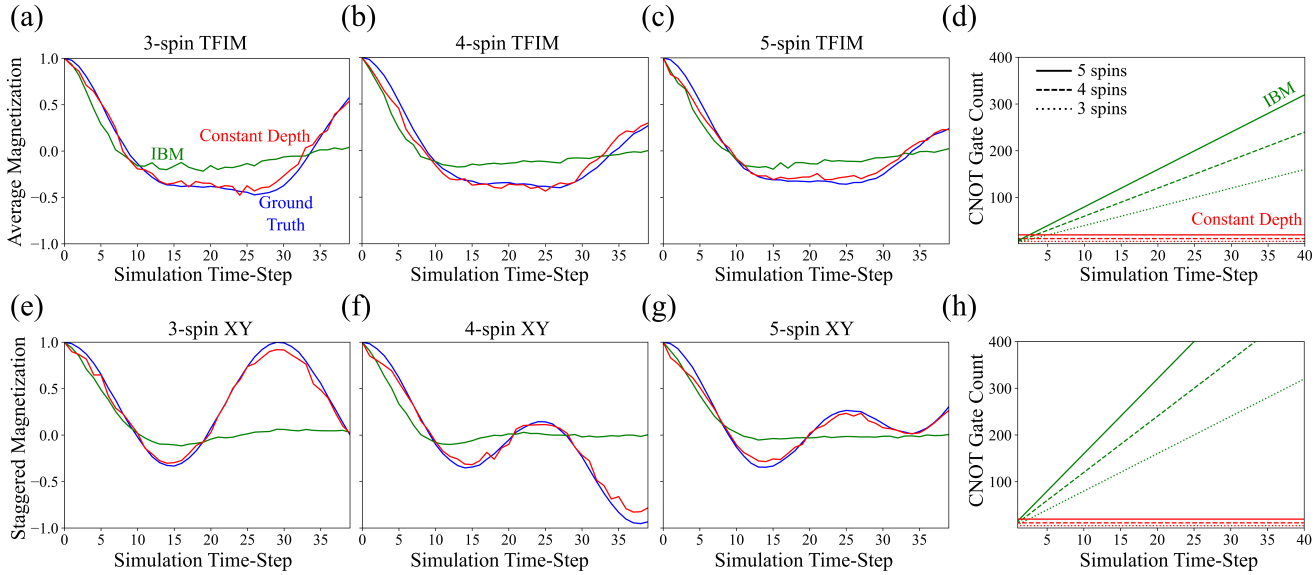

FIG. 3. Comparison of simulation results and CNOT gate count for the TFIM and XY model using the constant-depth circuits versus the IBM-compiled circuits. The top row shows simulation results for a TFIM with 3- (a), 4- (b), and 5-qubits (c). A noise-free simulator provides the ground truth, shown in blue, with which to compare results from the constant-depth circuits (red) and IBM-compiled circuits (green). The bottom row shows the analogous simulation results for the XY model with 3- (e), 4- (f), and 5-qubits (g). (d) and (h) show the number of CNOT gates in the constant-depth (red) and IBM-compiled (green) circuits for each time-step for 3- (dotted line), 4- (dashed line), and 5-qubit (solid line) systems for the TFIM and XY models, respectively.

per time-step for the XY model circuits (3h) are approximately double the number for the TFIM circuits (3d), while our constant-depth circuits have the same CNOT count for both models.

V. CONCLUSIONS

We have presented a method for generating circuits that are constant in depth with increasing numbers of time-steps for dynamic simulations of quantum materials. Our constant-depth circuits are currently applicable to one-dimensional Hamiltonian models with nearest-neighbor interactions along two or fewer axes, which we denote by $\mathcal{H}_{\mathcal{CD}}$. The constant-depth circuit structure for a system of size N has a number of CNOT gates that scales only quadratically with N. They are comprised of an array of two-qubit matchgates acting on nearest neighbor pairs of qubits. We find that the matchgates for the $\mathcal{H}_{\mathcal{CD}}$ Hamiltonians are special in that they can be decomposed into native-gate circuits requiring only two CNOT gates, as opposed to generic matchgates that require three. The ability to downfold circuits for dynamic simulation under $\mathcal{H}_{\mathcal{CD}}$ Hamiltonians to constant-depth relies on a set of conjectured identities for these special matchgates that we introduce in this paper. We demonstrate the power of the constant-depth circuits with dynamic simulations of the TFIM and XY models with 3-, 4-, and 5-qubits carried out on IBM's quantum processors. Our results illustrate how the constant-depth circuits enable successful dynamic simulations of quantum materials out to arbitrarily long times.

There are numerous directions for future investigations to explore whether constant-depth circuits can be created for various extensions including two-dimensional models, models with next-nearest neighbor or even longer-range interactions, or full Heisenberg interactions (i.e., interactions along three axes). Indeed, matchgates have previously been studied for various two-dimensional qubit topologies and for longer-range interactions [33, 34]. Paired with incremental improvements in quantum hardware, the ability to extend our constant-depth circuits to more complex systems would pave the way to new discoveries in the behavior of quantum materials by enabling long-time dynamic simulations of systems relevant to scientific and technological problems.

ACKNOWLEDGEMENTS

This work was supported by the U.S. Department of Energy (DOE) under Contract No. DE-AC02-05CH11231, through the Office of Advanced Scientific Computing Research Accelerated Research for Quantum Computing Program (LB, RVB, EY, CI, and WAdJ) and the Advanced Quantum Testbed (ES).

[1] F. Arute, K. Arya, R. Babbush, D. Bacon, J. C. Bardin, R. Barends, R. Biswas, S. Boixo, F. G. Brandao, D. A. Buell, *et al.*, Nature **574**, 505 (2019).

[2] J. Preskill, Quantum **2**, 79 (2018).

[3] P. W. Shor, SIAM Rev. **41**, 303 (1999).

[4] L. K. Grover, in *Proceedings 28th Annual ACM Symposium on the Theory of Computing* (ACM, 1996) pp. 212–219.

[5] R. P. Feynman, Int. J. Theor. Phys. **21**, 467 (1982).

[6] S. Lloyd, Science **273**, 1073 (1996).

[7] D. S. Abrams and S. Lloyd, Phys. Rev. Lett. **79**, 2586 (1997).

[8] C. Zalka, Proc. R. Soc. A **454**, 313 (1998).

[9] L. Bassman, M. Urbanek, M. Metcalf, J. Carter, A. F. Kemper, and W. A. de Jong, "Simulating quantum materials with digital quantum computers," (2021), arXiv:2101.08836.

[10] N. Wiebe, D. W. Berry, P. Høyer, and B. C. Sanders, J. Phys. A Math. Theor. **44**, 445308 (2011).

[11] A. Smith, M. S. Kim, F. Pollmann, and J. Knolle, npj Quantum Inf. **5**, 106 (2019).

[12] M. Möttönen, J. J. Vartiainen, V. Bergholm, and M. M. Salomaa, Phys. Rev. Lett. **93**, 130502 (2004).

[13] A. De Vos and S. De Baerdemacker, Phys. Rev. A **94**, 52317 (2016).

[14] R. Iten, R. Colbeck, I. Kukuljan, J. Home, and M. Christandl, Phys. Rev. A **93**, 032318 (2016).

[15] E. A. Martinez, T. Monz, D. Nigg, P. Schindler, and R. Blatt, New J. Phys. **18**, 063029 (2016).

[16] S. Khatri, R. LaRose, A. Poremba, L. Cincio, A. T. Sornborger, and P. J. Coles, Quantum **3**, 140 (2019).

[17] P. Murali, J. M. Baker, A. Javadi-Abhari, F. T. Chong, and M. Martonosi, in *Proceedings of the Twenty-Fourth International Conference on Architectural Support for Programming Languages and Operating Systems*, ASPLOS '19 (ACM, 2019) pp. 1015–1029.

[18] E. Younis, K. Sen, K. Yelick, and C. Iancu, "QFAST: Quantum Synthesis Using a Hierarchical Continuous Circuit Space," (2020), arXiv:2003.04462.

[19] L. Cincio, K. Rudinger, M. Sarovar, and P. J. Coles, "Machine learning of noise-resilient quantum circuits," (2020), arXiv:2007.01210.

[20] L. Bassman, S. Gulania, C. Powers, R. Li, T. Linker, K. Liu, T. K. S. Kumar, R. K. Kalia, A. Nakano, and P. Vashishta, Quantum Sci. Technol. **6**, 14007 (2020).

[21] A. Botea, A. Kishimoto, and R. Marinescu, in *Proceedings of the 11th International Symposium on Combinatorial Search (SoCS 2018)* (2018) pp. 138–142.

[22] D. Herr, F. Nori, and S. J. Devitt, npj Quantum Inf. **3**, 35 (2017).

[23] D. W. Berry, G. Ahokas, R. Cleve, and B. C. Sanders, Comm. Math. Phys. **270**, 359 (2007).

[24] A. M. Childs and R. Kothari, Quantum Inf. Comput. **10**, 669 (2010), 0908.4398.

[25] Y. Atia and D. Aharonov, Nat. Commun. **8**, 1572 (2017).

[26] C. Cîrstoiu, Z. Holmes, J. Iosue, L. Cincio, P. J. Coles, and A. Sornborger, npj Quantum Inf. **6**, 82 (2020).

[27] L. G. Valiant, SIAM J. Comput. **31**, 1229 (2002).

[28] G. Vidal and C. M. Dawson, Phys. Rev. A **69**, 10301 (2004).

[29] D. Poulin, A. Qarry, R. Somma, and F. Verstraete, Phys. Rev. Lett. **106**, 170501 (2011).

[30] H. F. Trotter, Proc. Amer. Math. Soc. **10**, 545 (1959).

[31] L. Bassman, K. Liu, A. Krishnamoorthy, T. Linker, Y. Geng, D. Shebib, S. Fukushima, F. Shimojo, R. K. Kalia, A. Nakano, *et al.*, Phys. Rev. B **101**, 184305 (2020).

[32] "Berkeley quantum synthesis toolkit," (2021), `https://bqskit.lbl.gov`.

[33] D. J. Brod and E. F. Galvão, Phys. Rev. A **86**, 52307 (2012).

[34] D. J. Brod and A. M. Childs, Quantum Inf. Comput. **14**, 901 (2014), 1308.1463.

Appendix A: Quantum circuits for $\mathcal{H}_{\mathcal{CD}}$ matchgates

CONSTANT DEPTH HEISENBERG: $J_xJ_y = J_xJ_z = J_yJ_z = 0$ AND $h_\beta = 0$

XX Matchgates

$$G := \begin{bmatrix} \cos\frac{\theta_1}{2} & & & -\mathtt{i}\sin\frac{\theta_1}{2} \\ & \cos\frac{\theta_1}{2} & -\mathtt{i}\sin\frac{\theta_1}{2} & \\ & -\mathtt{i}\sin\frac{\theta_1}{2} & \cos\frac{\theta_1}{2} & \\ -\mathtt{i}\sin\frac{\theta_1}{2} & & & \cos\frac{\theta_1}{2} \end{bmatrix} \tag{A1}$$

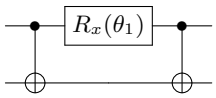

YY Matchgates

$$G := \begin{bmatrix} \cos\frac{\theta_1}{2} & & & \mathtt{i}\sin\frac{\theta_1}{2} \\ & \cos\frac{\theta_1}{2} & -\mathtt{i}\sin\frac{\theta_1}{2} & \\ & -\mathtt{i}\sin\frac{\theta_1}{2} & \cos\frac{\theta_1}{2} & \\ \mathtt{i}\sin\frac{\theta_1}{2} & & & \cos\frac{\theta_1}{2} \end{bmatrix} \tag{A2}$$

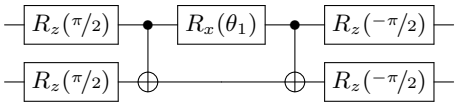

ZZ Matchgates

$$G := \begin{bmatrix} e^{-\frac{\mathtt{i}\theta_2}{2}} & & & \\ & e^{\frac{\mathtt{i}\theta_2}{2}} & & \\ & & e^{\frac{\mathtt{i}\theta_2}{2}} & \\ & & & e^{-\frac{\mathtt{i}\theta_2}{2}} \end{bmatrix} \tag{A3}$$

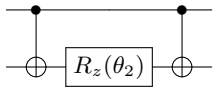

CONSTANT DEPTH HEISENBERG: $J_xJ_y = J_xJ_z = J_yJ_z = 0$ AND $h_\beta \neq 0$

XX + x Gates

$$G := \begin{bmatrix} \boldsymbol{a} & \boldsymbol{c} & \boldsymbol{c} & \boldsymbol{b} \\ \boldsymbol{c} & \boldsymbol{a} & \boldsymbol{b} & \boldsymbol{c} \\ \boldsymbol{c} & \boldsymbol{b} & \boldsymbol{a} & \boldsymbol{c} \\ \boldsymbol{b} & \boldsymbol{c} & \boldsymbol{c} & \boldsymbol{a} \end{bmatrix} \quad \begin{aligned} \boldsymbol{a} &= \left[\cos\tfrac{\theta_0}{2}\right]^2 \cos\tfrac{\theta_1}{2} + \mathtt{i}\left[\sin\tfrac{\theta_0}{2}\right]^2 \sin\tfrac{\theta_1}{2} \\ \boldsymbol{b} &= -\left[\sin\tfrac{\theta_0}{2}\right]^2 \cos\tfrac{\theta_1}{2} - \mathtt{i}\left[\cos\tfrac{\theta_0}{2}\right]^2 \sin\tfrac{\theta_1}{2} \\ \boldsymbol{c} &= -\tfrac{1}{2}\mathtt{i}e^{-\frac{\mathtt{i}\theta_1}{2}} \sin\theta_0 \end{aligned} \tag{A4}$$

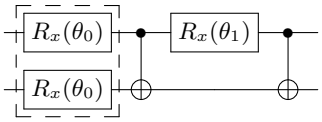

YY + y Gates

$$G := \begin{bmatrix} \boldsymbol{a} & \boldsymbol{d} & \boldsymbol{d} & -\boldsymbol{b} \\ -\boldsymbol{d} & \boldsymbol{a} & \boldsymbol{b} & \boldsymbol{d} \\ -\boldsymbol{d} & \boldsymbol{b} & \boldsymbol{a} & \boldsymbol{d} \\ -\boldsymbol{b} & -\boldsymbol{d} & -\boldsymbol{d} & \boldsymbol{a} \end{bmatrix} \quad \boldsymbol{d} = -\mathtt{i}\boldsymbol{c} \tag{A5}$$

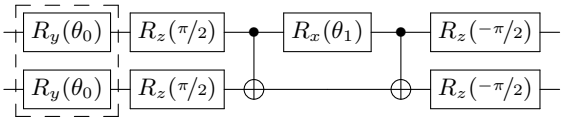

ZZ + z Matchgates

$$G := \begin{bmatrix} e^{-\frac{\mathtt{i}\theta_2}{2}-\mathtt{i}\theta_0} & & & \\ & e^{\frac{\mathtt{i}\theta_2}{2}} & & \\ & & e^{\frac{\mathtt{i}\theta_2}{2}} & \\ & & & e^{-\frac{\mathtt{i}\theta_2}{2}+\mathtt{i}\theta_0} \end{bmatrix} \tag{A6}$$

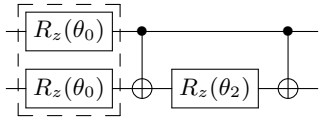

CONSTANT DEPTH HEISENBERG: $J_xJ_yJ_z = 0$ AND $h_\beta = 0$

XY Matchgates

$$G := \begin{bmatrix} \cos\frac{\theta_1-\theta_2}{2} & & & -\mathtt{i}\sin\frac{\theta_1-\theta_2}{2} \\ & \cos\frac{\theta_1+\theta_2}{2} & -\mathtt{i}\sin\frac{\theta_1+\theta_2}{2} & \\ & -\mathtt{i}\sin\frac{\theta_1+\theta_2}{2} & \cos\frac{\theta_1+\theta_2}{2} & \\ -\mathtt{i}\sin\frac{\theta_1-\theta_2}{2} & & & \cos\frac{\theta_1-\theta_2}{2} \end{bmatrix} \tag{A7}$$

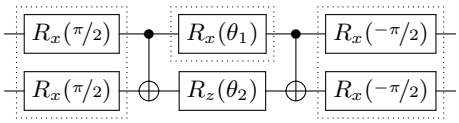

XZ Matchgates

$$G := \begin{bmatrix} e^{-\frac{\mathtt{i}\theta_2}{2}}\cos\frac{\theta_1}{2} & & & -\mathtt{i}e^{-\frac{\mathtt{i}\theta_2}{2}}\sin\frac{\theta_1}{2} \\ & e^{\frac{\mathtt{i}\theta_2}{2}}\cos\frac{\theta_1}{2} & -\mathtt{i}e^{\frac{\mathtt{i}\theta_2}{2}}\sin\frac{\theta_1}{2} & \\ & -\mathtt{i}e^{\frac{\mathtt{i}\theta_2}{2}}\sin\frac{\theta_1}{2} & e^{\frac{\mathtt{i}\theta_2}{2}}\cos\frac{\theta_1}{2} & \\ -\mathtt{i}e^{-\frac{\mathtt{i}\theta_2}{2}}\sin\frac{\theta_1}{2} & & & e^{-\frac{\mathtt{i}\theta_2}{2}}\cos\frac{\theta_1}{2} \end{bmatrix} \tag{A8}$$

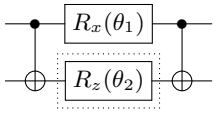

YZ Matchgates

$$G := \begin{bmatrix} e^{-\frac{\mathtt{i}\theta_2}{2}}\cos\frac{\theta_1}{2} & & & \mathtt{i}e^{-\frac{\mathtt{i}\theta_2}{2}}\sin\frac{\theta_1}{2} \\ & e^{\frac{\mathtt{i}\theta_2}{2}}\cos\frac{\theta_1}{2} & -\mathtt{i}e^{\frac{\mathtt{i}\theta_2}{2}}\sin\frac{\theta_1}{2} & \\ & -\mathtt{i}e^{\frac{\mathtt{i}\theta_2}{2}}\sin\frac{\theta_1}{2} & e^{\frac{\mathtt{i}\theta_2}{2}}\cos\frac{\theta_1}{2} & \\ \mathtt{i}e^{-\frac{\mathtt{i}\theta_2}{2}}\sin\frac{\theta_1}{2} & & & e^{-\frac{\mathtt{i}\theta_2}{2}}\cos\frac{\theta_1}{2} \end{bmatrix} \tag{A9}$$

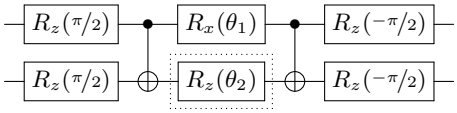

CONSTANT DEPTH HEISENBERG: $J_xJ_yJ_z = 0$ AND $h_\beta \neq 0$

(XX + z) and (YY + z) and (XY + z) Matchgates

$$G := \begin{bmatrix} e^{-\mathtt{i}(\theta_0+\theta_3)}\cos\frac{\theta_1-\theta_2}{2} & & & -\mathtt{i}e^{\mathtt{i}(\theta_0-\theta_3)}\sin\frac{\theta_1-\theta_2}{2} \\ & \cos\frac{\theta_1+\theta_2}{2} & -\mathtt{i}\sin\frac{\theta_1+\theta_2}{2} & \\ & -\mathtt{i}\sin\frac{\theta_1+\theta_2}{2} & \cos\frac{\theta_1+\theta_2}{2} & \\ -\mathtt{i}e^{-\mathtt{i}(\theta_0-\theta_3)}\sin\frac{\theta_1-\theta_2}{2} & & & e^{\mathtt{i}(\theta_0+\theta_3)}\cos\frac{\theta_1-\theta_2}{2} \end{bmatrix} \tag{A10a}$$

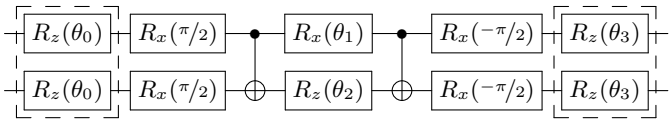

(A10b)

(XX + y) and (ZZ + y) and (XZ + y) Gates

$$G := \begin{bmatrix} e & g & g & f \\ -\overline{g} & \overline{e} & -\overline{f} & \overline{g} \\ -\overline{g} & -\overline{f} & \overline{e} & \overline{g} \\ f & -g & -g & e \end{bmatrix} \tag{A11a}$$

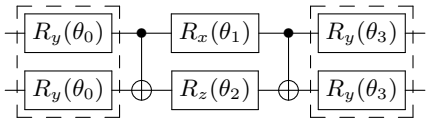

$$\begin{aligned} e &= \tfrac{1}{2}\left[\cos\tfrac{\theta_1+\theta_2}{2} + \cos\tfrac{\theta_1-\theta_2}{2}\cos(\theta_0+\theta_3)\right] - \tfrac{1}{2}\mathtt{i}\left[\sin\tfrac{\theta_1+\theta_2}{2} - \sin\tfrac{\theta_1-\theta_2}{2}\cos(\theta_0-\theta_3)\right] \\ f &= \tfrac{1}{2}\left[\cos\tfrac{\theta_1+\theta_2}{2} - \cos\tfrac{\theta_1-\theta_2}{2}\cos(\theta_0+\theta_3)\right] - \tfrac{1}{2}\mathtt{i}\left[\sin\tfrac{\theta_1+\theta_2}{2} + \sin\tfrac{\theta_1-\theta_2}{2}\cos(\theta_0-\theta_3)\right] \\ g &= -\tfrac{1}{2}\cos\tfrac{\theta_1-\theta_2}{2}\sin(\theta_0+\theta_3) - \tfrac{1}{2}\mathtt{i}\sin\tfrac{\theta_1-\theta_2}{2}\sin(\theta_0-\theta_3) \end{aligned} \tag{A11b}$$

(YY + x) and (ZZ + x) and (YZ + x) Gates

$$G := \begin{bmatrix} e & h & h & -f \\ -\overline{h} & \overline{e} & -\overline{f} & -\overline{h} \\ -\overline{h} & -\overline{f} & \overline{e} & -\overline{h} \\ -f & h & h & e \end{bmatrix} \qquad h = \mathtt{i}g \tag{A12}$$

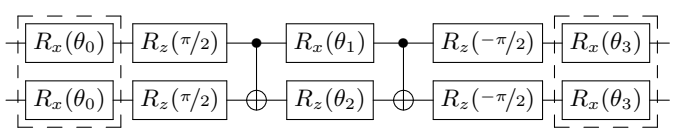

Appendix B: Proof of Fig. 1a

Proof. Using (11) recursively, yields

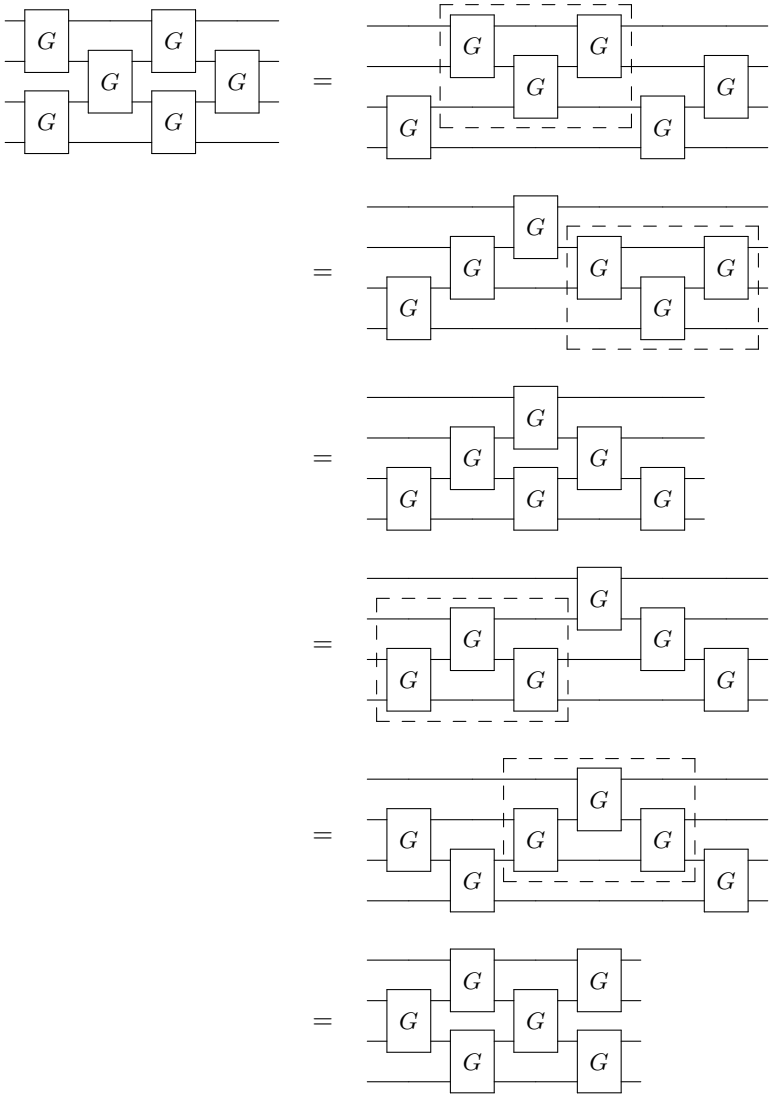

□